Poroelastic stressing and induced seismicity near the Lacq gas field, southwestern France

Paul Segall

Department of Geophysics, Stanford University, Stanford, California

Jean-Robert Grasso

Laboratoire de Géophysique Interne et Tectonophysique, Observatoire de Grenoble, Grenoble France

Antony Mossop

Department of Geophysics, Stanford University, Stanford, California

Abstract. Hundreds of shallow, small to moderate earthquakes have occurred near the Lacq deep gas field in southwestern France since 1969. These earthquakes are clearly separated from tectonic seismicity occurring in the Pyrenees, 25 km to the southwest. The induced seismicity began when the reservoir pressure had declined by $\sim$ 30 MPa. Repeated leveling over the field shows localized subsidence reaching a maximum of 60 mm in 1989. Segall (1989) suggested that poroelastic stressing, associated with volumetric contraction of the reservoir rocks, is responsible for induced seismicity associated with fluid extraction. To test this model, we compare the observed subsidence and hypocentral distributions with the predicted displacement and stress fields. We find that the relationship between average reservoir pressure drop and subsidence is remarkably linear, lending support to the linear poroelastic model. Displacements and stresses are computed based on a priori knowledge of the reservoir geometry, material properties, and reservoir pressure changes. The computed vertical displacements are found to be in excellent agreement with the subsidence observed from leveling. Stress perturbations accompanying gas extraction, computed using the same parameters, are found to be $\sim$ 0.2 MPa or less. Changes in Coulomb failure stress are computed assuming that slip occurs on optimally oriented planes. The predicted failure zones correlate very well with the spatial distribution of earthquakes if the perturbing stresses are small in comparison to the ambient regional deviatoric stresses and if the minimum regional compressive stress axis is vertical. Accurate determination of focal mechanisms of the induced events would allow a more rigorous test of the poroelastic model and could lead to important inferences about the crustal stress state.

Introduction

There is increasing evidence that the extraction of pore fluids can trigger seismic activity [*Yerkes and Castle*, 1976; *Pennington et al.*, 1986; *Wetmiller*, 1986; *Grasso and Wittlinger*, 1990]. *Segall* [1989] summarized the observations from a number of active oil and gas fields and suggested that the induced earthquakes are caused by poroelastic stressing associated with fluid withdrawal. One of the best documented cases of seismicity induced by extraction of pore fluids is the Lacq gas field in southwestern France [*Grasso and Wittlinger*, 1990; *Feignier and Grasso*, 1990; *Grasso and Feignier*, 1990; *Guyoton et al.*, 1992].

In this paper we compute the stress and deformation fields induced by gas extraction in the Lacq area. We test the poroelastic model by comparing the vertical displacement field predicted by forward calculations with subsidence observed by repeated leveling. The forward calculations are based on the known geometry of the Lacq field and measured pore pressure changes within the reservoir. We find that the predicted displacements are in good agreement with the measured subsidence. This suggests that the stresses computed from the poroelastic model are reasonably accurate. We then compare the locations of the Lacq earthquakes with those predicted by the poroelastic model using a simple Coulomb failure condition.
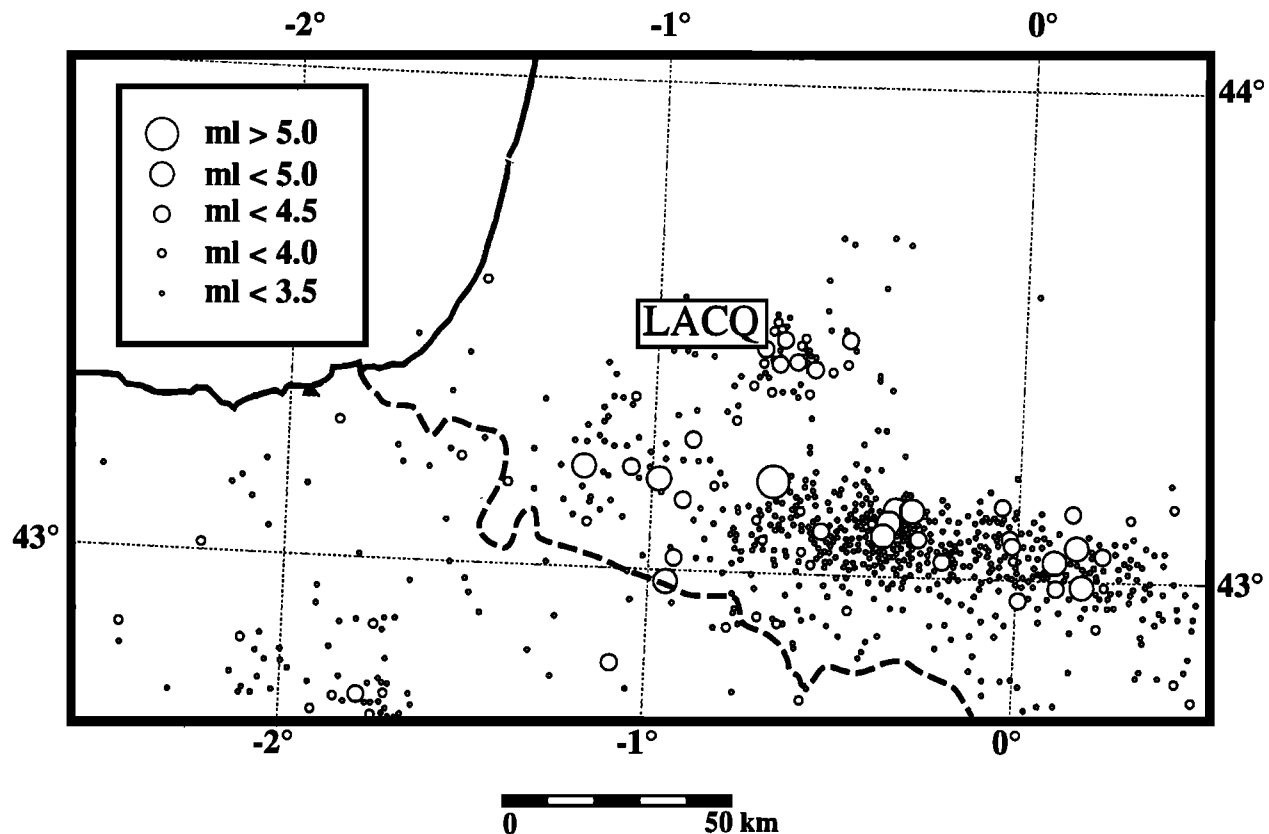
Observations

Seismicity

Figure 1 illustrates regional seismicity in southwestern France between 1962 and 1990 located by the French

PYRENEAN SEISMIC ACTIVITY (1962-1990)

Figure 1. Seismicity in the Pyrenees 1962-1990 located by the French National Network. Horizontal location accuracies are 3-5 kilometers for $M > 3$ events.

National network. The distinct band of seismicity running WNW-ESE through the central part of the figure is associated with the main Pyrenean Fault. The north Pyrenean foreland is generally aseismic, with the exception of a tight cluster of events northwest of the city of Pau. This cluster, which has been active since 1969, is located in the Lacq area, the site of the largest gas field in France.
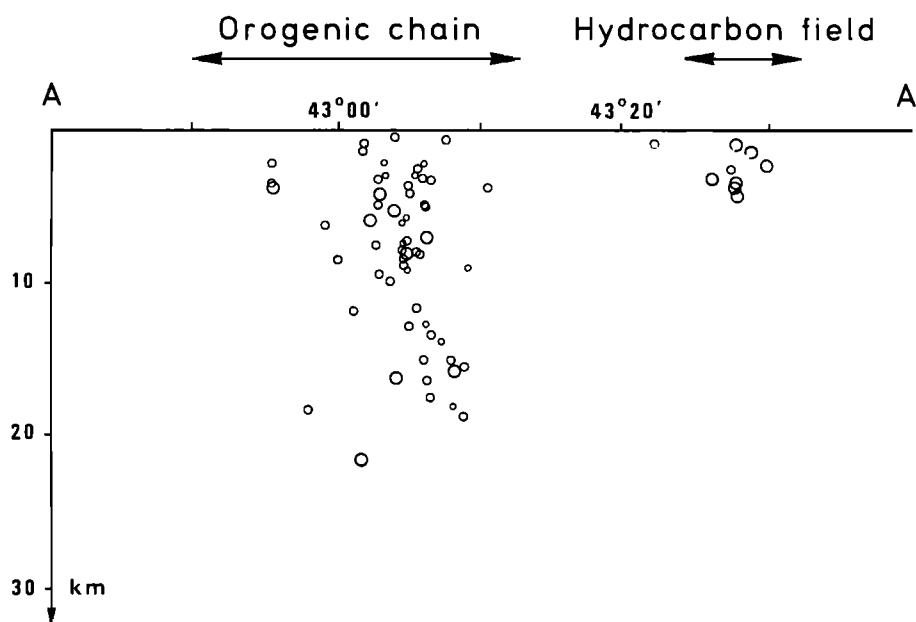
A vertical cross section through the region emphasizes the separation between the Pyrenean earthquakes and the Lacq seismicity. Figure 2 illustrates seismicity during October to December 1982 located with a temporary network [*Gallart et al.*, 1985]. Each event is located with at least 20 stations, and the location accuracy is approximately 1 km. It is clear from Figure 2 that the Lacq seismicity is separated by 25 km from the Pyrenean belt and is much shallower than tectonic seismicity to the southwest.

Earthquakes recorded by a local network installed in the vicinity of the Lacq gas field show that virtually all of the earthquake epicenters occur within the gas field [*Grasso and Wittlinger*, 1990]. The local telemetered network was installed in 1974 with four stations. The number of stations increased to 7 (one 3-component) between 1976 and 1981. A downhole seismometer was installed at 3,200 m depth in 1981. Unfortunately, because of corrosion of the cable, only one component

worked, and this only for 2 years. In 1990 a temporary network of 9 additional single-component stations was operated to aid in determining focal mechanisms. In 1991, three 3-component accelerometers were installed in the area to determine ground motions caused by local earthquakes. In 1992 the network was expanded and now includes 14 single-component seismometers, one 3-component seismometer, and three accelerometers.

Figure 3 illustrates the distribution of earthquakes located by the local network using an a priori three-dimensional velocity model based on seismic reflection profiles, vertical seismic profiles, and borehole data [*Guyoton et al.*, 1992]. The spatial association of the epicenters and the gas field is quite striking. From cross sections of the seismicity (Figure 4) it is clear that the earthquakes are closely associated with the gas reservoir.

It should be pointed out that the focal depths are not particularly well constrained. *Grasso and Wittlinger* [1990] used events recorded between 1976 and 1979 in a coupled inversion for velocity and hypocentral locations. They found that most of the seismicity had occurred above the gas reservoir. Locations based on the three-dimensional velocity model of *Guyoton et al.* [1992] generally fall below the gas reservoir. In Figure 4 we show seismicity between 1976 and 1979 and between 1982 and 1992, as located with the *Guyoton et al.* [1992] veloc-

Figure 2. North-south vertical cross section of seismicity through the Pyrenees between October to December 1982. North is to the right in the figure. All events are located with at least 20 arrivals. Location accuracy is approximately 1 km. After *Gallart et al.* [1985].

ity model. Note that when all the events are located with the same velocity model, there is no evidence for an increase in focal depth with time.

Petroleum Production

A shallow oil field was discovered in the Lacq area in 1949. Oil is produced from Upper Cretaceous limestones at 640-700 m depth. By 1986, cumulative oil production was 4×10^6 m^3 [*Nicolai et al.*, 1992]. Pore pressure in the oil reservoir has not changed greatly over time (Figure 5). The initial pressure in 1950 was 6.1 MPa, and pressure decreased to 5.9 MPa by 1954. Between 1954 and 1975, 10^7 m^3 of water were injected into the oil reservoir, causing pressures to rise to 6.5 MPa by 1975. Subsequently, pressure declined to 6.2 MPa by 1989.

In 1951 a gas condensate reservoir, ten times larger than the shallow oil reservoir, was discovered at a depth of 3,500 m. Production began in 1957 from Upper Jurassic and Lower Cretaceous carbonates that are overlain by impermeable shales and marls. The structure is a northwest-trending anticlinal dome (Figure 4) with a culmination at a depth of 3200 m. The southwest limb of the fold is faulted, while the northeast flank dips gently at 10°-20° from the top of the dome.

The gas reservoir contains two producing zones [*Nicolai et al.*, 1992]. The upper level consists of Lower Cretaceous carbonates of very low porosity, between 0.1% and 6%. The lower level consists of Upper Jurassic dolomites up to 200 m thick. The average porosity of the upper 100 m of the dolomites is 5-6%, decreasing to 0.1% at the base. The effective reservoir thickness is between 250 and 450 m, with average porosity of 3.5%. Matrix permeability is everywhere very low, 0.1 to a few millidarcies, but is enhanced by a high density of fractures.

The gas was initially highly overpressured; initial reservoir pressure in 1957 was 66.1 MPa (at 3700 m depth below sea level). Since that time, production has caused the pore pressure to decline dramatically (Figure 5). The pore pressure distribution over the central portion of the field has been remarkably uniform, with pressure differences between wells throughout the field of only a few tenths of MPa (Figure 5). This attests to the high fracture permeability in the central part of the reservoir. During the early stages of production, the observed pressure volume relationship behaved as if the pore volume was constant, indicating no recharge, and leading to the notion of a "sealed chamber" [*Nicolai et al.*, 1992]. We interpret this to imply that the fracture permeability decreases dramatically on the flanks of the dome structure. In fact, measured transmissivities range from in excess of 10,000 mdarcy-m in the central region to 50 - 500 mdarcy-m on the northern flank of the structure. Numerical models [*de Lanlay*, 1990] show that in order to fit the observed pressure the permeability must decrease from 500 mdarcy near the culmination of the dome at 3200 m to 10 mdarcy at a depth of 4800 m, and 0.035 mdarcy at 5800 m depth. Recognizing that the pressure was very nearly constant over the central portion of the reservoir led to the concentration of production to the center of the dome and the abandonment of wells along the flanks of the structure.

Wastewater has been injected into the deep gas reservoir beginning in 1975, 6 years after the first earthquakes in the area. Between 1975 and 1989, 3.3×10^6 m^3 was injected into the southern flank of the dome. The effect of this injection may have been to isolate a small pocket of gas from the surrounding reservoir. While this pocket is at a somewhat higher pressure than the surrounding reservoir, the gas pressure there in 1990
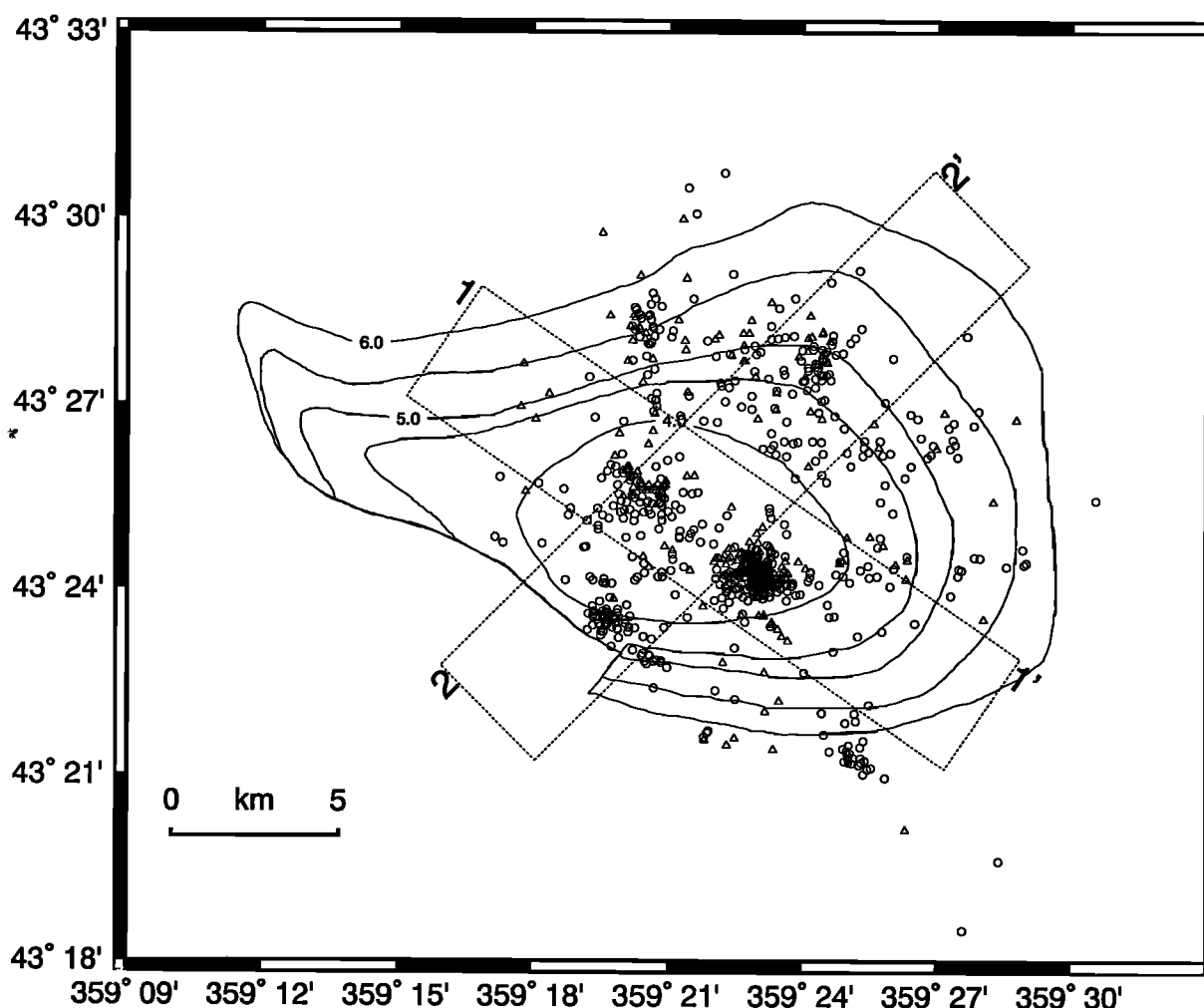
Figure 3. Earthquakes located by a local network compared to the extent of the gas field. Locations are based on the velocity model of *Guyoton et al.* [1992] . Triangles represent epicenters between 1976 and 1979, and circles, 1982 to 1992. Contours indicate depth to the top of the gas reservoir. Boxes show locations and width of cross sections shown in Figure 4.

was still 50 MPa less than the initial, preproduction pressure.

Figure 5 also compares the temporal history of seismicity with pore pressures in the oil and gas reservoirs. By far the most significant physical change is the dramatic decrease in pressure within the gas reservoir. Pressure changes within the shallow oil reservoir are 2 orders of magnitude less than the pressure changes in the gas reservoir. The first earthquake was recorded in 1969 at a time when the gas pressure had decreased by ∼ 30 MPa. It is important to note that $M \geq 3$ earthquakes at Lacq are felt. A search of historical records [*Grasso and Wittlinger,* 1990] showed that there were no reported felt earthquakes prior to the 1969 event. Since 1969, there have been several felt earthquakes per year. In conclusion, there is clearly both a temporal and spatial relationship between the seismicity and the gas production.

While there is a possibility of a temporal correlation between injection in the shallow oil reservoir and seismicity, we do not believe shallow injection is a signifi-

cant factor in causing the earthquakes for the following reasons: (1) The spatial distribution of epicenters is comparable to the extent of the gas reservoir but much wider than the oil field [*Grasso and Wittlinger,* 1990]. (2) At the time of the first earthquakes (1969) both the oil and gas reservoir pressures had decreased from the ambient preproduction pressures. Furthermore, the maximum oil field pressure changes are only 1% of the gas reservoir pressure changes. (3) Most of the earthquakes occurred below the low-permeability marls that cap the gas reservoir and thus could not be hydraulically connected to the shallow reservoir. Since the marls have sealed the gas reservoir over geologic time, it is clear that they are impermeable on the timescale of a few decades. We conclude that the gas pressure changes dominate the induced seismicity. However, it is possible that injection in the shallow oil field could be a factor in some of the very shallowest earthquakes.

Leveling Data

There are two leveling lines that cross over the Lacq field that provide valuable information on the subsi-

Depth Section 1 - 1'

Depth Section 2 - 2'
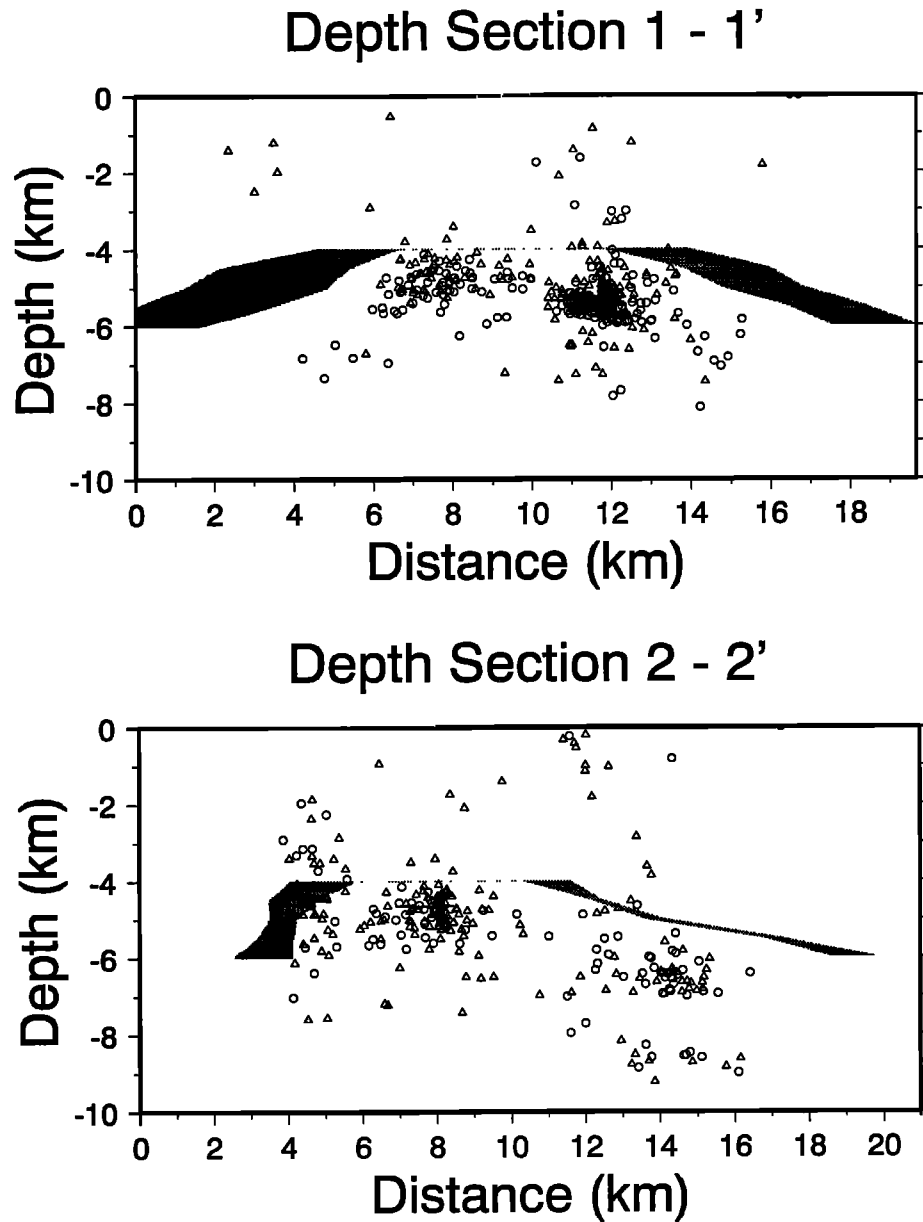
Figure 4. Vertical cross sections through the Lacq dome showing the relationship between the seismicity and the gas reservoir. Triangles represent epicenters between 1976 and 1979, and circles, 1982 to 1992. Location of sections is shown in Figure 3. Shaded zone is the top of the reservoir. Thickness represents variation in the depth to the top of the reservoir across the breadth of the section. (top) Northwest–southeast section and (bottom) Southwest–northeast section.
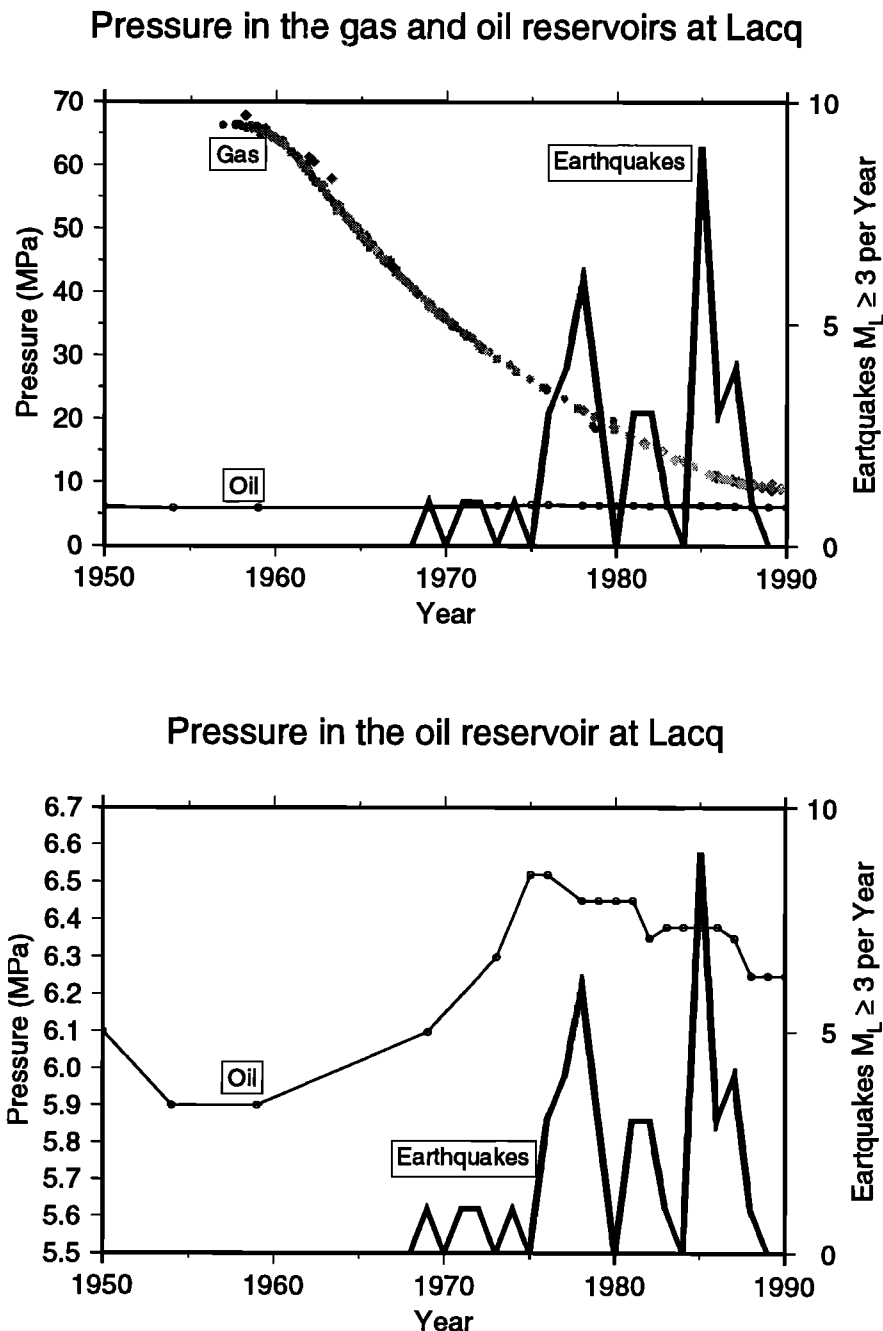
dence accompanying production. A northwest-southeast trending line has been repeatedly leveled and provides important constraints on the deformation associated with fluid extraction. The line was first leveled in 1887, well before any hydrocarbon production. It was releveled in 1967 (to first-order, double-run standards), 1979 (first order, single run), and in 1989 and 1990. Elevation changes are illustrated in Figure 6. The 1979 leveling shows a down-to-the-southeast tilt of roughly 1 part per million, suggesting some form of systematic error. The tilt has been removed from the data shown in Figure 6.

Theory

We review here the methods used for computing stress alterations due to fluid extraction as given by *Segall* [1992]. This work builds upon earlier results of *Geertsma* [1966, 1973].

The approach is based on the theory of linear poroelasticity [*Biot*, 1941; *Rice and Cleary*, 1976]. For an isotropic poroelastic medium, the solid volume strain ϵ_{kk} is related to changes in mean stress $\sigma_{kk}/3$ and pore pressure p by

$$\epsilon_{kk} = \frac{\sigma_{kk}}{3K} + \frac{\alpha p}{K} \qquad (1)$$

Pressure in the gas and oil reservoirs at Lacq



Pressure in the oil reservoir at Lacq

Figure 5. Pressure history within the Lacq oil and gas fields. (top) Oil and gas field pressure (left scale) and histogram of earthquakes located within the field with magnitudes greater than 3.0 (right scale). Gas pressures in various monitoring wells are shown with different symbols. (bottom) Oil field pressure on expanded scale.

where K is the undrained bulk modulus and α is the Biot pore pressure coefficient. The Biot coefficient is restricted to the range $0 \le \alpha \le 1$ and is generally an increasing function of porosity. Equation (1) shows that if the reservoir were free from constraints ($\sigma_{kk} = 0$), it would contract by an amount $\alpha p/K$ as the pore pressure decreased. On the other hand, if the reservoir were perfectly constrained ($\epsilon_{kk} = 0$), it would be driven into tension $\sigma_{kk} = -3\alpha p$. In actuality, the rocks surrounding the reservoir provide an incomplete constraint, the reservoir shrinks by some amount less than

$\alpha p/K$, is driven into tension, and the surrounding rocks are stressed.

In general, the deformation and pore pressure fields are coupled through the equilibrium equations for the solid and the equation governing pore fluid flow. Rather than attempt to solve for the pore pressure distribution as a function of space and time, we will use field measurements and reservoir simulations to determine the reservoir pressure.

If the pore pressure field is known, then the displacements and stresses can be computed from a distribu-
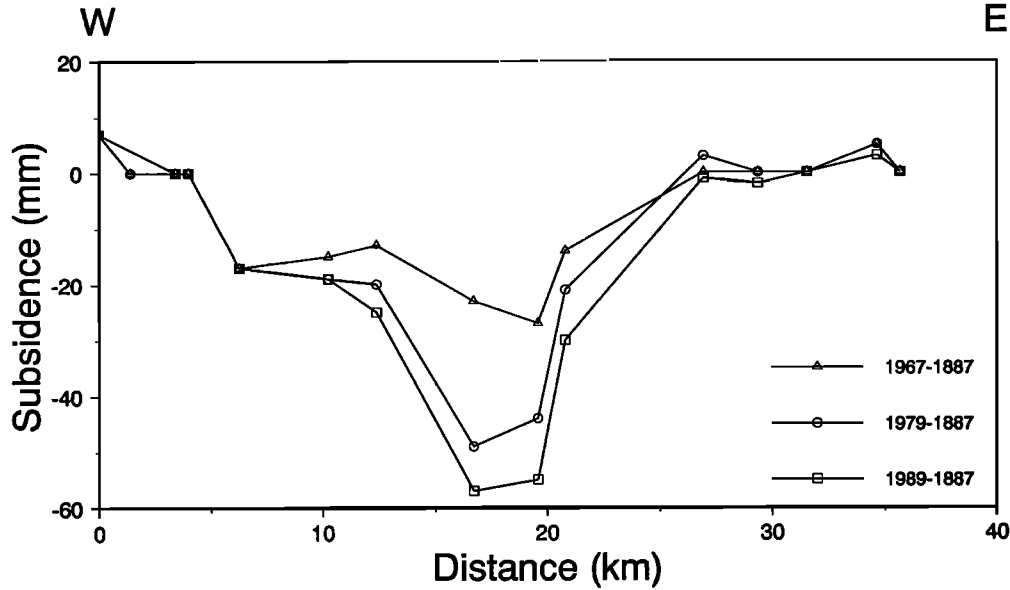
Figure 6. Elevation changes determined by repeated leveling over the Lacq field along a roughly northwest-southeast profile.

tion of centers of dilatation with strengths proportional to $\alpha p(\mathbf{x})$ [*Geertsma*, 1966]. The reservoir at Lacq is roughly axisymmetric, so we consider cases in which the pore pressure changes due to production depend only on radial distance and depth, $p(r, z)$. The displacements due to an arbitrary axisymmetric pressure distribution are

$$u_i(r, z) = \frac{\alpha}{\mu} \int_0^\infty \int_0^\infty p(\rho, d) g_i(r, z; \rho, d) d\rho dd, \qquad (2)$$

where μ is the shear modulus. The Green's functions, $g_i(r, z; \rho, d)$, correspond to a ring of dilatation at radius ρ and depth d and are given by *Segall* [1992]

$$g_r(r, z) = \frac{(1 - 2\nu)}{2(1 - \nu)} \frac{\rho}{2} \int_0^\infty k J_1(kr) J_0(k\rho)[e^{\epsilon k(z-d)}$$
$$+ e^{-k(z+d)}(3 - 4\nu - 2kz)] dk \qquad (3)$$

and

$$g_z(r, z) = -\frac{(1 - 2\nu)}{2(1 - \nu)} \frac{\rho}{2} \int_0^\infty k J_0(kr) J_0(k\rho)[\epsilon e^{\epsilon k(z-d)}$$
$$+ e^{-k(z+d)}(3 - 4\nu + 2kz)] dk \qquad (4)$$

where ν is Poisson's ratio. For computational purposes, equations (3) and (4) are written in terms of elliptic integrals using relations given by *Eason et al.* [1955].

Given the displacements, the stresses are computed from the strains and the poroelastic constitutive equations. Because the stress Green's functions are singular, it is computationally advantageous to integrate by parts and write the integrals in terms of the pore pressure gradients,

$$\sigma_{ij}(r, z) = \alpha \frac{(1 - 2\nu)}{2(1 - \nu)} \times$$
$$\int_0^\infty \int_0^\infty \frac{\partial p(\rho, d)}{\partial \rho} G_{ij}(r, z; \rho, d) d\rho dd - p\delta_{ij}, \qquad (5)$$

where the kernels G_{ij} are related to the displacement Green's functions via

$$G_{ij} = \frac{\partial g_i}{\partial x_j} + \frac{\partial g_j}{\partial x_i} + \frac{2\nu}{1 - 2\nu} \frac{\partial g_k}{\partial x_k} \delta_{ij} \qquad (6)$$

The functions $G_{ij}(r, z; \rho, d)$ are given in terms of elliptic integrals by *Segall* [1992].

Comparison of Model and Data

The theory is linear and therefore predicts a linear relationship between pore pressure decline in the reservoir and surface displacement (see equation (2)). In fact, if we compare the maximum observed surface subsidence with gas pressure decline, we see that the relationship is very nearly linear (Figure 7). This gives us consider-
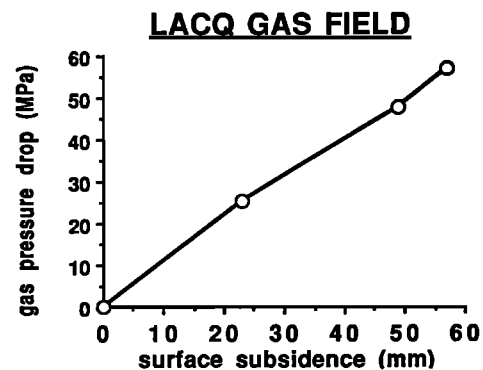
Figure 7. Maximum observed subsidence compared with reservoir pressure decline. The poroelastic model predicts a linear relationship, consistent with the observations.

able confidence in applying the linear poroelastic model. There is no evidence in these data for plastic yielding, which would be characterized by a decrease in the slope of the pressure subsidence curve. Furthermore, the data are consistent with the pressure change occurring in a reservoir of constant size.

The inverse slope of the line in Figure 7 is roughly 1 mm MPa^{-1}. We can test whether this is consistent with the theory using a simplified reservoir model. For this calculation we will assume that the reservoir pressure decline is uniform within a disk of radius R and that the thickness of the reservoir T is small in comparison to its depth d, as in the work by *Geertsma* [1973]. We thus take the pressure distribution to be

$$p(\rho, z) = \Delta p H(R - \rho) \qquad d - \frac{T}{2} \le z \le d + \frac{T}{2}$$
$$p(\rho, z) = 0 \qquad\qquad \text{otherwise} \tag{7}$$

where $H(x)$ is the Heavyside function. Using the results from the previous section, we find the displacements at the Earth's surface are

$$u_z(r, 0) = -\frac{\alpha(1 - 2\nu)T\Delta p}{\mu} \times$$
$$\int_0^R \rho d\rho \int_0^\infty k J_0(kr) J_0(k\rho) e^{-kd} dk \tag{8}$$

Exchanging the order of integration and noting that

$$\int \rho J_0(k\rho) d\rho = k^{-1}\rho J_1(k\rho), \tag{9}$$

we find that

$$u_z(r, 0) = -\frac{\alpha(1 - 2\nu)T\Delta p}{\mu} R \int_0^\infty J_0(kr) J_1(kR) e^{-kd} dk, \tag{10}$$

which recovers equation (26) of *Geertsma* [1973]. The maximum displacement at $r = 0$ is found from the asymptotic form of (10) as $r/R \to 0$ [*Eason et al.*, 1955]

$$u_z(0, 0) = -\frac{\alpha(1 - 2\nu)T\Delta p}{\mu}[1 - \frac{d/R}{\sqrt{(1 + (d/R)^2)}}]. \tag{11}$$

In order to test the simplified model against the data, we need to have representative values for the material properties and geometric characteristics of the reservoir. Shear modulus and Poisson's ratio have been determined from laboratory tests on core samples from the Lacq field. The various lithologies exhibit Young's moduli ranging from 22 GPa to 64 GPa [*Grasso and Feignier*, 1990]. In the calculations, we use a Young's modulus of 60 GPa, representative of the carbonate reef, since this unit makes up the bulk of the rock mass overlying the reservoir. It is also one of the stiffest units as determined by the laboratory data. For this reason,

and because the core samples exclude macroscopic fractures, the value we use may somewhat overestimate the in situ stiffness. The corresponding shear modulus with a Poisson's ratio of 0.25 is 23 GPa (Table 1).

To determine the Biot coefficient α of the reservoir rocks, we used laboratory measurements of the change in pore volume induced by a change in confining pressure at constant (atmospheric) pore pressure,

$$C_{pc} = -\frac{1}{V_p} \left(\frac{\partial V_p}{\partial P_{conf}}\right)_p \tag{12}$$

where V_p is the pore volume, P_{conf} is confining pressure, and p is pore pressure. The notation indicates that the pore pressure is held constant as the confining pressure is varied. The reciprocal theorem and superposition principle can be employed to show that for homogeneous isotropic solid constituents with fully connected pore space, $\alpha = \phi K C_{pc}$ (appendix), where ϕ is porosity and K is undrained bulk modulus. From the laboratory data on a single sample of reservoir rock [*Vidal*, 1988], we determine that $\phi = 2 \times 10^{-3}$, $K = 1.6 \times 10^5$ bar, and $C_{pc} = 1.45 \times 10^{-4}$ bar^{-1}. This yields $\alpha = 5 \times 10^{-2}$.

This result alone would not be particularly useful, since this sample is from one of the lowest porosity (0.2%) carbonates present in the gas reservoir. However, together with published data for limestones of differing porosities, it allows us to estimate the Biot coefficient with some confidence. *Laurent et al.* [1990] measured α for three limestones with porosities of 4.5%, 14.5%, and 23%. The Biot coefficient α was measured by determining the ratio of change in pore volume to the change in bulk volume at fixed pore pressure.

Recall that α is expected to be an increasing function of porosity. *Laurent et al.* [1990] found empirically that α has a power law dependence on porosity. Remarkably, the value of α we determined for the extremely low porosity limestone sample from the Lacq reservoir falls right on the trend (Figure 8) of the higher porosity samples analyzed by *Laurent et al.* [1990]. This allows us to interpolate and determine a value of α for the average reservoir rocks within the Lacq reservoir. For typical porosities of 0.02 to 0.04, we estimate that $0.2 < \alpha < 0.3$. For the purpose of the following calculations we will take $\alpha = 0.25$ (Table 1).

The geometric and material parameters are summarized in Table 1. The one remaining parameter that is imperfectly known is the reservoir thickness T. Although the net reservoir thickness is roughly 450 m, the effective thickness is perhaps as low as 250 m because

Table 1. Parameters Used in Calculations

Symbol	Quantity	Value
α	Biot Coefficient	0.25
ν	Poisson's Ratio	0.25
μ	Shear Modulus	2.3×10^4 MPa
Δp	Pressure Decline	60 MPa
T	Reservoir Thickness	250 m
d	Reservoir Depth	3.5 km
R	Reservoir Radius	7.0 km
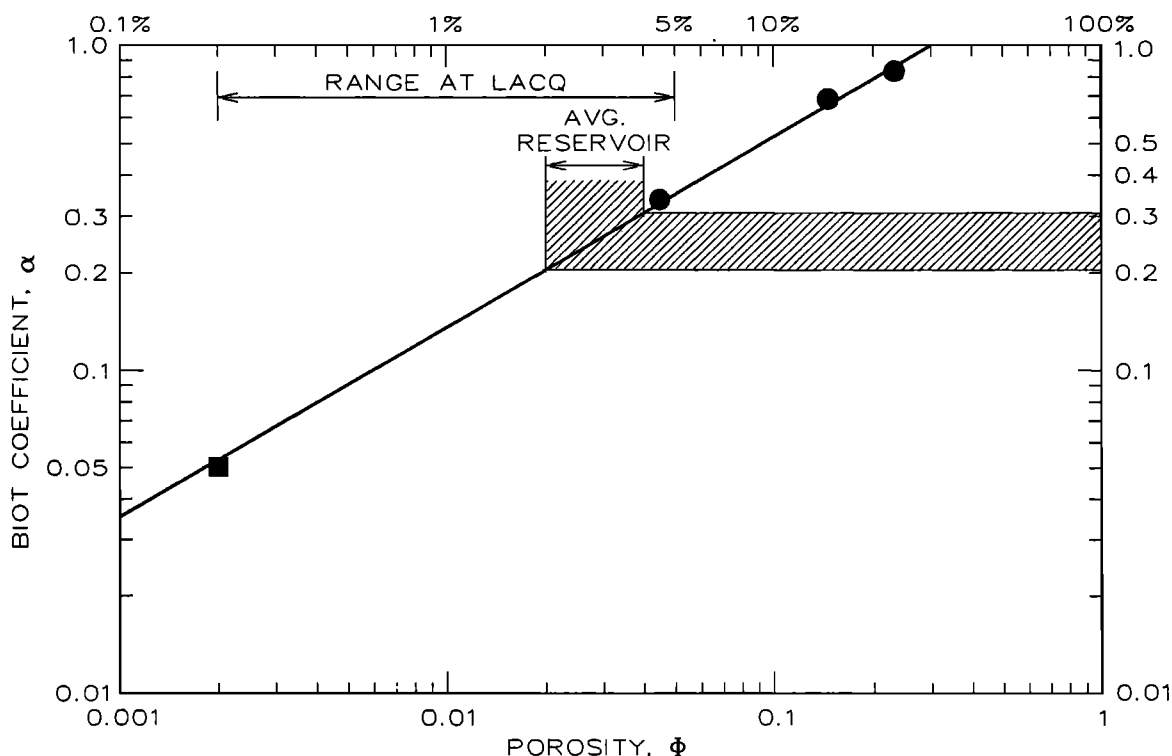
Figure 8. Biot coefficient α as a function of porosity for several limestone samples. Circles indicate average values determined by *Laurent et al.* [1990] for the Lavoux ($\phi = 0.23$), Vilhonneur ($\phi = 0.145$), and Larrys Mouchete ($\phi = 0.045$) limestones. The square indicates the value estimated here for the lowest porosity limestones within the Lacq gas reservoir. The hatch-marked interval represents typical porosities of limestones within the Lacq gas reservoir.

of porosity variations within the reservoir. Using these values as a range for T, we estimate a subsidence rate, from equation (11), of between 0.7 mm MPa^{-1} for T = 250 m and 1.3 mm MPa^{-1} for T = 450 m. These values bracket the observed rate of 1.0 mm MPa^{-1} extremely well, especially when one considers the uncertainties in the parameters, particularly α, μ, and ϕ.

We next compare the pattern of vertical displacements determined from repeated leveling with that predicted by the poroelastic model. The reservoir pressure change is known reasonably well from in situ measurements and reservoir simulations. For our limited purposes the reservoir pressure distribution can be assumed to be axisymmetric. As was discussed above, the pore pressures within the central reservoir are very nearly uniform, presumably because of the great fracture permeability near the apex of the anticlinal dome. Reservoir pressures increase rapidly near the periphery of the reservoir. In fact, the distribution of pore pressure change inferred from reservoir simulation models [*de Lanlay*, 1990] is reasonably approximated as

$$p(r,t) = p_0(t)e^{-(\frac{r}{r_c})^4}, \qquad (13)$$

where $p_0(t)$ is the maximum pressure decline at $r = 0$, and r_c is the characteristic radius of the reservoir. With uniform hydraulic properties the width of the pressure drawdown zone would be predicted to expand with time. Because of the extremely nonuniform distribu-

tion of permeability, this expansion is slow and can be safely neglected here.

By integrating the pressure decline given by equation (13) against the displacement Green's functions, we can predict a priori the surface displacements and compare them with results from repeated leveling. In this calculation, r_c is taken to be 8.0 km, while the reservoir thickness is adjusted slightly, to 300 m, in order to better fit the maximum subsidence. The maximum pressure drop at the time of the leveling is 55 MPa. The comparison between the observed and predicted subsidence is shown in Figure 9. In general, the theoretically predicted displacements are in good agreement with observations.

There is a tendency for the observed subsidence to be more concentrated near the center of the field. A possible explanation for this is that we have approximated the reservoir as flat-lying and neglected the domal structure. Fortunately, this is very easily accommodated in the present analytical scheme. From structural contour maps on the top of the gas reservoir we approximate the depth to the reservoir as

$$d(r) = d_0 - A[e^{-(\frac{r}{l_c})^2} - \frac{1}{2}], \qquad (14)$$

where A is the amplitude of the dome and l_c is the characteristic length of the structure. The predicted surface displacements are shown for a dome with amplitude of 1.4 km and a width l_c of 5.0 km in Figure 9.
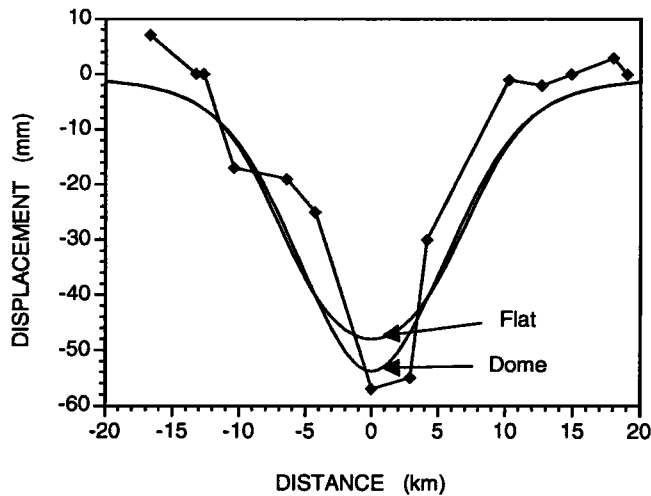
Figure 9. Predicted vertical displacements at Lacq compared to leveling results for the time interval 1887–1989. Two predicted models are shown: one modeling the reservoir as a flat layer, and the second including the effect of the anticlinal dome structure.

The effect of bringing the center of the field closer to the surface does concentrate the deformation slightly, somewhat improving the fit to the data.

Stress Changes

Given the success of the poroelastic model in predicting the surface subsidence, we are encouraged to calculate the perturbations to the preexisting stress field due to fluid extraction. We then compare the predicted stress changes to the spatial distribution of seismicity.

The effective mean normal stress, $I_1 = (\hat{\sigma}_1 + \hat{\sigma}_2 + \hat{\sigma}_3)/3$, is shown in the top panel of Figure 10. The $\hat{\sigma}_i$ are the effective principal stresses, where effective stress for deformation is defined as $\hat{\sigma}_{ij} = \sigma_{ij} + \alpha p \delta_{ij}$. In this calculation we take the response of the rock outside the reservoir to be drained ($\Delta p = 0$), so that the effective stress and total stress are the same, except within the reservoir. The undrained pore pressure response would be simply calculated from $\Delta p = -B\sigma_{kk}/3$, where B is the Skempton's pore pressure coefficient. The effective mean normal stress change is compressive above and below the reservoir and slightly tensile on the flanks of the reservoir. The magnitudes of the stress perturbations are quite modest, reaching a maximum of 0.2 MPa (2 bars) at the surface. Note that the total stress, as compared to the effective stress, exhibits a large tension within the reservoir of magnitude $\alpha p(\mathbf{x})$. This occurs because the contraction of the reservoir is resisted by the elastic surroundings, as discussed previously. The
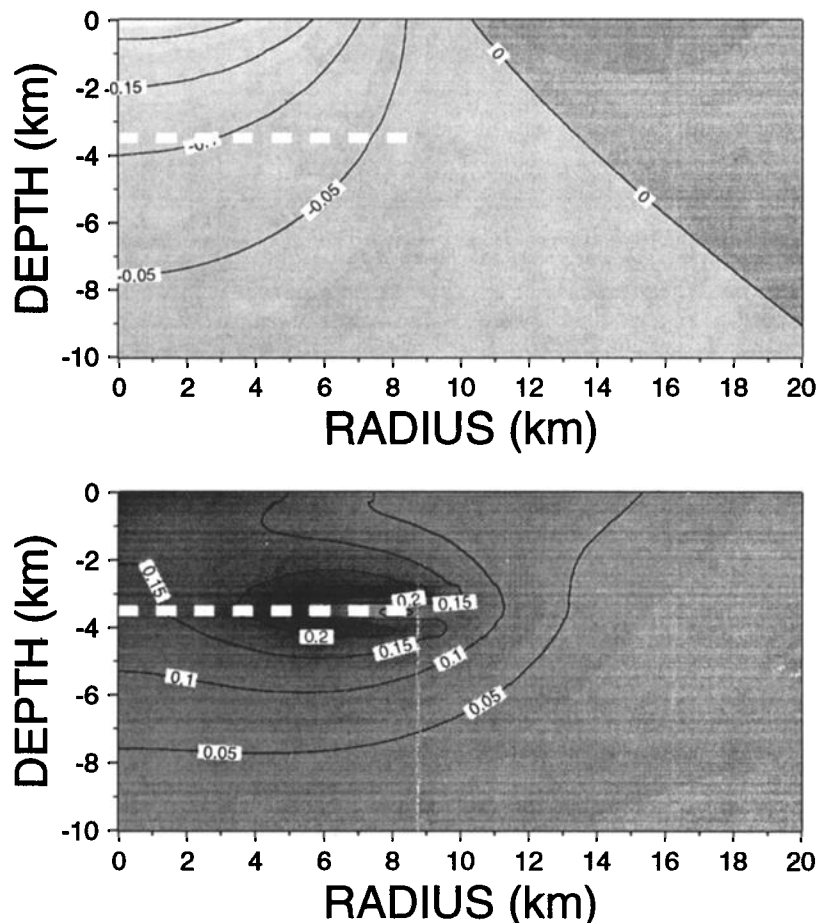
Figure 10. Predicted stress change around the Lacq reservoir due to poroelastic stressing. (top) Effective mean normal stress (in megapascals), and (bottom) maximum shear stress (in in megapascals). Parameters are as given in Table 1. Dashed white line outlines the model gas reservoir.

stress changes within the reservoir are of the order of 15 MPa; however their effect on frictional stability is mitigated by the large reductions in pore pressure.

The maximum shear stress, given by the square-root of the second deviatoric stress invariant ($[[(\sigma_1 - \sigma_3)^2 + (\sigma_1-\sigma_2)^2+(\sigma_2-\sigma_3)^2]/6)^{\frac{1}{2}}$ is shown in the bottom panel of Figure 10. The shear stress is strongly concentrated near the edge of the reservoir where the maximum pore pressure gradients occur. The maximum shear stress change outside the reservoir is approximately 0.2 MPa.

To compute the effect of these stress perturbations on seismicity, we adopt a simple Coulomb failure criterion. Slip on a plane occurs when $|\tau| \geq \eta\sigma_n$, where τ and σ_n are the shear and normal tractions (compression positive) and η is the coefficient of friction. Whether or not a fault slips, as well as the direction of slip, depends on the total stress (the sum of the regional, preproduction stress state and the perturbing poroelastic stresses), the fault orientation, and the coefficient of friction η. In the calculations here we use a value of $\eta = 0.75$; however, the results do not qualitatively change for the range of values typically found for rock, $0.5 < \eta < 0.8$. We assume, for the moment, that there are faults available with similar coefficients of friction at all orientations.

Because the poroelastic stresses are no larger than ~ 0.2 MPa, we begin by assuming that the perturbing shear stresses are very small compared to the preexisting stress differences. This means that the orientation of the fault planes most likely to slip is governed by the preexisting regional stress field. The regional principal stress orientations are assumed to be constant throughout the region, whereas the perturbing stress field has radial symmetry. Thus the total stress is not radially symmetric and the predicted failure zones will depend on azimuth.
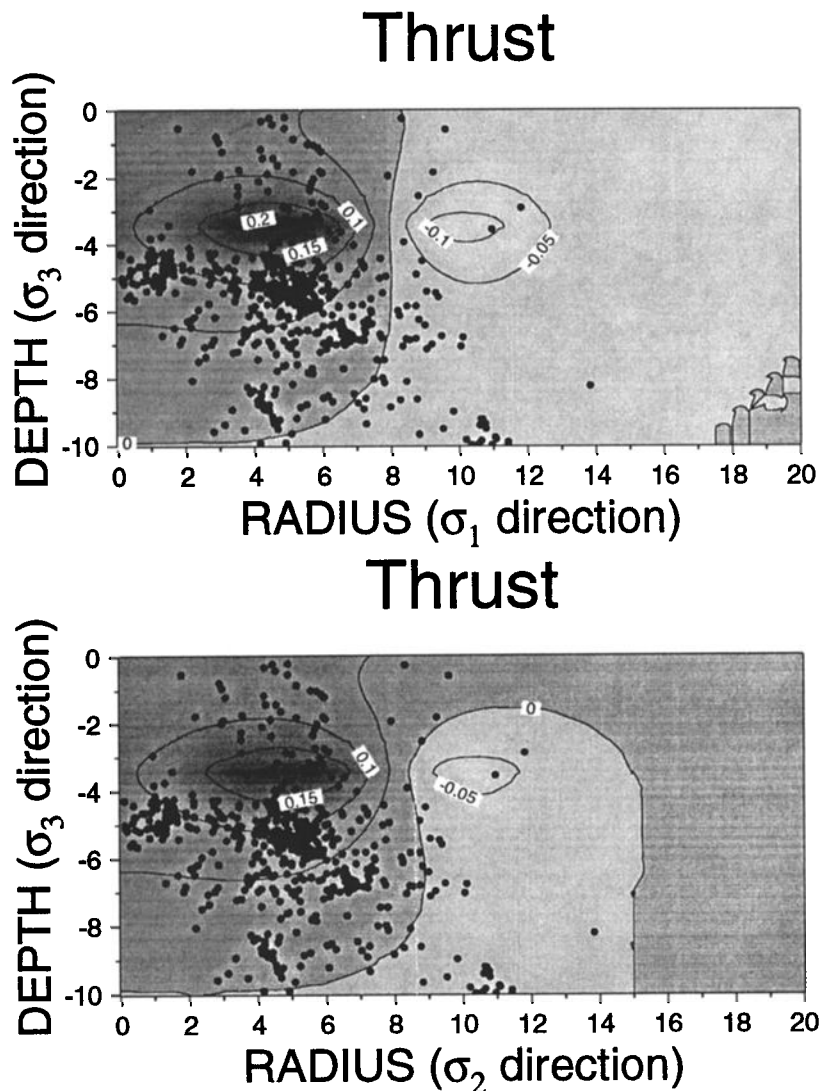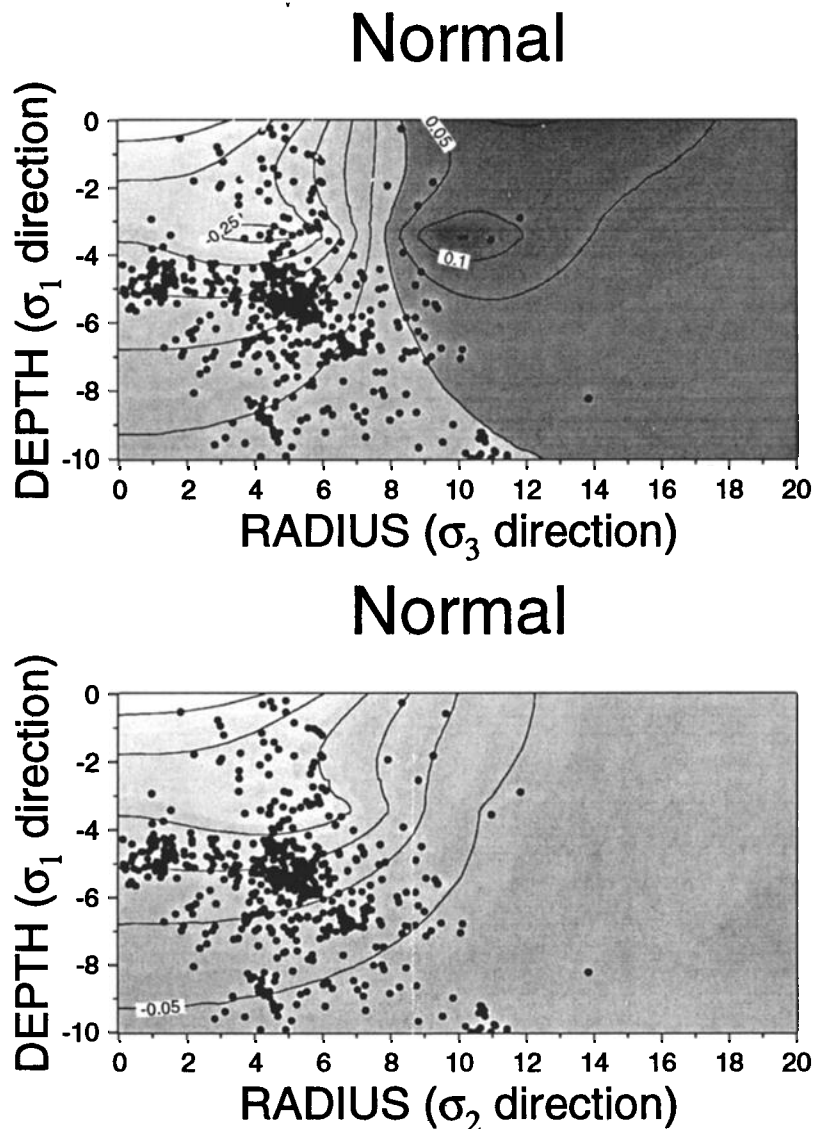

Figure 11. Vertical cross sections comparing Coulomb failure stress (in megapascals) with earthquake locations for a regional thrusting environment. Coefficient of friction is $\eta = 0.75$. Dark shading indicates the region where gas withdrawal promotes reverse slip on optimally oriented planes; light shading indicates the region where withdrawal inhibits reverse slip. Earthquake locations are projected circumferentially onto a vertical plane. (top) Plane perpendicular to the intermediate stress, σ_2 direction. (bottom) Plane perpendicular to the maximum compression, σ_1 direction.

The result for a thrusting regime, that is, one in which the least principal stress σ_3 is vertical, is shown in Figure 11. The result for a normal regime, vertical σ_1, is shown in Figure 12. In these figures we show the change in Coulomb failure condition, $\Delta|\tau| - \eta\Delta\sigma_n$, across faults optimally oriented for failure with respect to the regional stress. Here, $\Delta|\tau|$ is the perturbation in the shear traction in the direction of slip, and $\Delta\sigma_n$ is the perturbation in compression. The upper plots show vertical cross sections parallel to the σ_1-σ_3 plane, the lower plots show vertical cross sections perpendicular to the σ_1-σ_3 plane. Also plotted are earthquakes locations from *Guyoton et al.* [1992] projected circumferentially onto a vertical plane through an estimated center of the reservoir (43°26'N, 0°40'W). The dark regions show areas where the change in Coulomb condition favors slip on optimally oriented planes, whereas the light areas show regions where the change in Coulomb condition inhibits slip. We would expect the earthquakes to plot in the dark zones, and indeed, the correlation between hypocenter locations and the predicted failure zone is quite good for the thrust case (Figure 11). It is worth noting that including the anticlinal structure in the calculations would cause the maximum Coulomb stress to be deeper and thus closer to the majority of the earthquakes. While the Coulomb stress fits the observed locations fairly well for the thrusting case, for a normal stress regime (Figure 12) the Coulomb stress is nearly anticorrelated with the earthquake locations. The strike slip case (not shown) also exhibits a poor correlation with the distribution of earthquakes.

Figure 13 compares the Coulomb stress with the seismicity in a horizontal section at a depth of 4.5 km. The σ_1 direction was chosen to be perpendicular to the Pyre-

Figure 12. Vertical cross sections comparing Coulomb failure stress (in megapascals) with earthquake locations for a regional normal faulting environment. Coefficient of friction is $\eta = 0.75$. Dark shading indicates the region where gas withdrawal promotes normal slip on optimally oriented planes; light shading indicates the region where withdrawal inhibits normal slip. Earthquake locations are projected circumferentially onto a vertical plane. (top) Plane perpendicular to the intermediate stress, σ_2 direction. (bottom) Plane perpendicular to the minimum compression, σ_3 direction.

Thrust (σ_3 vertical, σ_1 N45°E)
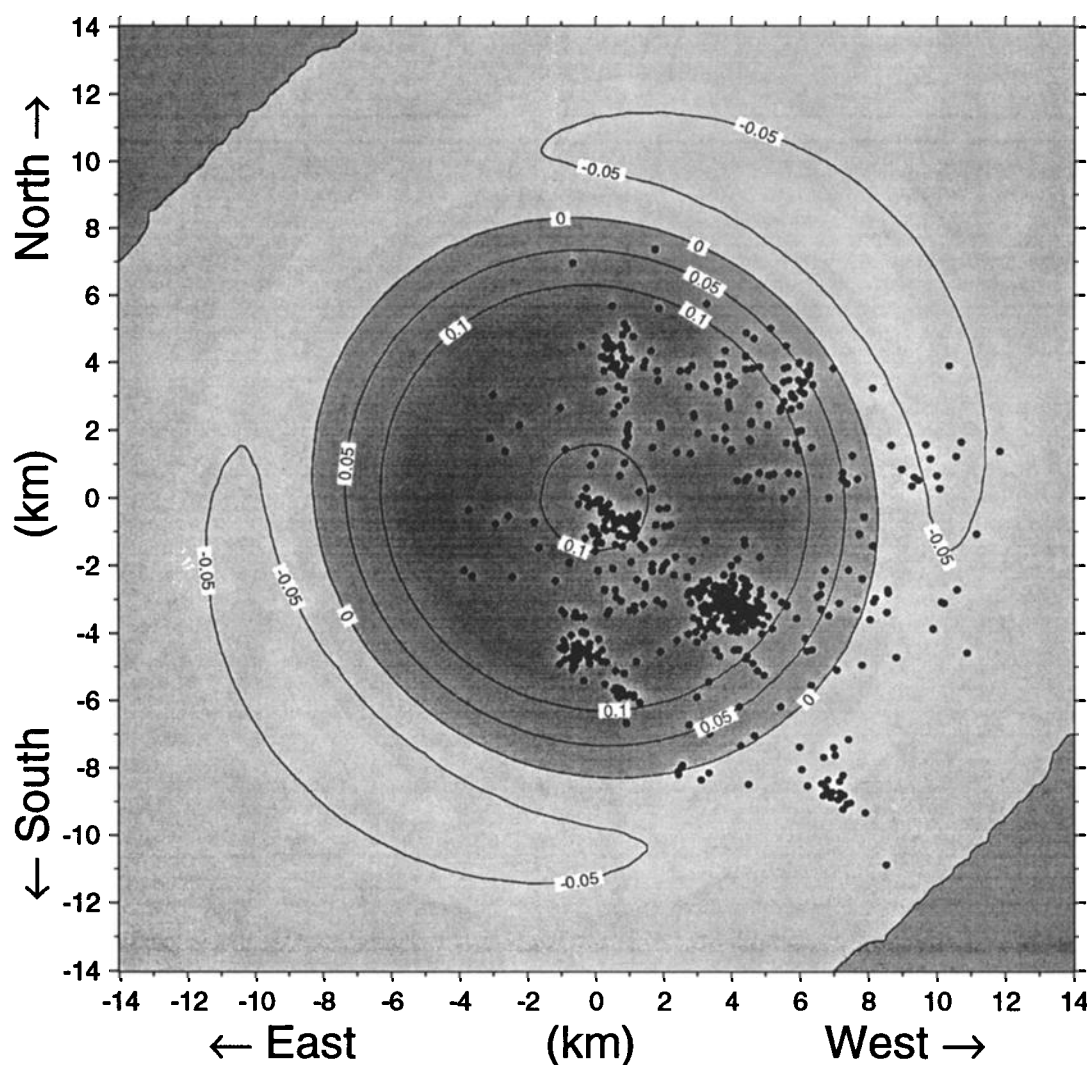
Figure 13. Horizontal section at a depth of 4.5 km comparing Coulomb failure stress (in megapascals) with earthquake locations for a thrust faulting environment. Coefficient of friction is $\eta = 0.75$. Dark shading indicates the region where gas withdrawal promotes reverse slip; light shading indicates the region where withdrawal inhibits reverse slip. The σ_1 direction was chosen to be perpendicular to the Pyrenees.

nees, an orientation consistent with regional tectonics. It should be pointed out, however, that the Coulomb stress distribution is so nearly circular that this hardly influences the comparison. We conclude that given our previous assumptions, the poroelastic stresses predict the distribution of earthquakes reasonably well, assuming that the regional least compressive stress is vertical.

Even for the thrust faulting case, there are a number of earthquakes that plot within the zone of decreased Coulomb stress (Figures 11 and 13). This could be due to a poor estimate of the reservoir center or a lack of radial symmetry in the structure. The discrepancies could also be due to elastic heterogeneity or to preexisting zones of weakness in certain orientations. Both possibilities are discussed below.

Ideally, we would use the focal mechanisms of the earthquakes to independently determine the orienta-

tion of the principal stress axes from stress inversions [e.g., *Gephart and Forsyth*, 1984] and compare these with our results based on the spatial distribution of the seismicity. If the stress inversions showed vertical σ_3, this would further support the poroelastic model of induced seismicity. Unfortunately, the seismic network at Lacq has generally been too sparse to determine robust focal mechanisms. Indeed, there have been conflicting results on the focal mechanisms in the area, depending on the velocity model used and, perhaps, the time interval considered. Composite focal mechanisms based on the *Grasso and Wittlinger*, [1990] velocity model display predominantly reverse slip, indicating that the minimum regional stress is approximately vertical [*Feignier and Grasso*, 1990]. However, as discussed previously, focal depths based on the three-dimensional velocity model of *Guyoton et al.* [1992] are significantly greater

than those of *Feignier and Grasso* [1990], substantially altering the takeoff angles and thus the computed mechanisms. Mechanisms determined with the later velocity model show many normal events for the period 1976 to 1986, and a preponderance of reverse mechanisms since that time *Volant* [1993]. We conclude that the inferences based on focal mechanisms are, at present, not sufficient to test our interpretation that the least principal stress is vertical.

Up to this point we have assumed that slip occurs on optimally oriented planes. This is equivalent to assuming that preexisting planes of weakness exist at all orientations. If, on the other hand, slip is confined to preexisting planes of weakness at certain orientations, then the distribution of the Coulomb failure condition will be modified. For example, it is possible to find reasonable agreement between the predicted Coulomb failure condition and the observed distribution of seismic events in a normal regional stress field if the faults are constrained to lie approximately 60° from vertical, some 30° shallower than optimum. However, without independent evidence that weak planes of this orientation actually exist, it is difficult to support this interpretation.

A further complicating factor is heterogeneity in elastic structure. Laboratory tests as well as in situ velocity measurements demonstrate considerable variability in elastic stiffness. One expects stress to be concentrated in the stiffer lithologic units. Finite element calculations (D.F. McTigue, et al., unpublished calculations) do show considerable concentration of stress in the carbonate reef above the reservoir. The overall stress distribution is, however, quite similar to that found in the homogeneous models presented here. Unfortunately, much less is known about elastic properties below the reservoir. Given the uncertainty in the earthquake depth determinations, we feel that the simple model provides an adequate basis for comparing poroelastic effects with seismicity. More realistic models may become useful as the data quality improves.

For completeness we consider the other end-member model, in which the deviatoric components of the perturbing stresses are large in comparison to the regional deviatoric stress. Given the small magnitude of the poroelastic stresses, this essentially means that the preexisting stress would have to have been isotropic. The small stress perturbations could have induced the seismicity only if the pore pressures were nearly lithostatic. Drilling data clearly shows that this is not the case in the carbonate reef overlying the reservoir, where rather low pore pressures were encountered. However, we have no direct data on pore pressures below the reservoir, other than to note that initial pore pressures within the reservoir were near lithostatic.

In the limit that the regional deviatoric stress vanishes, the orientation of the optimal slip planes varies with position. The Coulomb stress in this limit is shown in Figure 14. As expected, the highest Coulomb stresses are located near the edge of the reservoir, where the shearing is maximal. The orientation of the optimal failure planes is shown with the simulated focal mech-

anisms. We again assume a coefficient of friction, η, of 0.75. The orientations of the slip planes with respect to the maximum compression, given by $\frac{1}{2}\tan \eta^{-1}$, would not vary by more than a few degrees for $0.5 < \eta < 0.8$. For a purely isotropic initial stress the faulting ranges from thrusting in the central region to predominantly strike slip off the flanks of the reservoir. There is an intermediate region, $r \sim 8$ km, in which one potential slip plane is reverse and the other low-angle normal, and even a small zone where both planes exhibit normal slip.

Discussion

We conclude from the preceding discussion that a more thorough test of the poroelastic model will only be possible with accurate fault plane solutions and/or in situ stress measurements. With well-constrained focal mechanisms we could rigorously test the model by asking whether the stress perturbations act to increase the tendency for slip in the observed slip direction. Furthermore, it may be possible to place constraints on the ratio of the regional to perturbing deviatoric stresses. In the limit that the perturbing stresses are small, then the stress inferred from the mechanisms of the induced events would tend to be spatially uniform. Systematic variations in the inferred stress field around the gas reservoir could then constrain the ratio of the perturbing to regional stresses. Since the perturbing stresses can be calculated from the known reservoir pressure changes, this then places some constraints on the magnitude of the regional deviatoric stress magnitudes. This could then be compared with in situ measurements.

An implication of our results is that the seismicity at Lacq was triggered by rather small stress changes. We compute Coulomb stress alterations of up to 0.2 MPa near the margin of the reservoir. These stresses correspond to reservoir pressure declines of 60 MPa, whereas the seismicity began in 1969 when the reservoir pressure had dropped by 30 MPa. This means that Coulomb stress changes of 0.1 MPa or less were capable of triggering earthquakes. Of course, locally steeper pore pressure gradients or other factors could lead to local stress concentrations (discontinuous changes in reservoir pore pressure yield singularities in stress); however, these local stress concentrations would be expected to attenuate rapidly with distance from the reservoir. While the magnitude of these stress changes may appear to be small, other studies of induced seismicity, resulting, for example, from reservoir filling, find stress changes of a similar magnitude as those reported here [e.g., Roeloffs, 1988]. Correlations between aftershock activity and the quasi-static mainshock induced stress changes suggest that stress changes as small as 0.01–0.05 MPa can trigger seismicity [*Reasenberg and Simpson*, 1992; *Stein et al.*, 1992]. These results imply that much of the crust is at incipient frictional failure and that this is true even in areas not associated with recent seismicity or tectonism.

Small Regional Stress
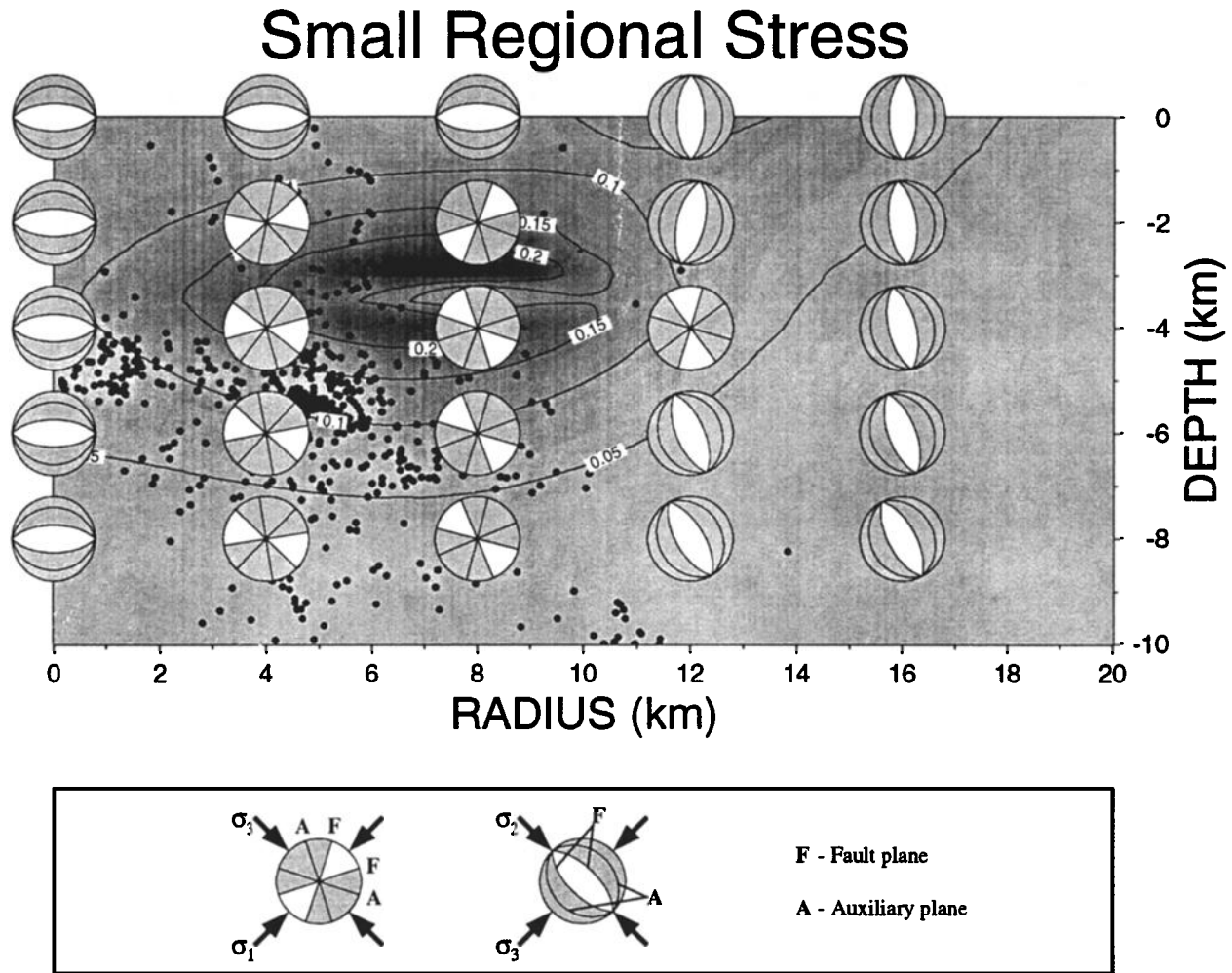
Figure 14. Vertical cross section comparing Coulomb failure stress (in megapascals) with locations of earthquakes for a purely isotropic regional stress. Coefficient of friction is $\eta = 0.75$. Also shown are simulated focal mechanisms (lateral hemispheres facing the observer) predicted by the Coulomb criterion for the computed stress field. For a given stress state there are two possible mechanisms, both of which are shown. The inset shows the relationship between the principal stress directions and the two possible fault planes, **F**, and their associated auxiliary planes, **A**. The unshaded part of the focal sphere experiences dilational first motions for either mechanism.

Conclusion

The simple linear poroelastic model provides a good quantitative prediction of the surface subsidence. There is no evidence for inelastic yielding in the displacement pressure change history. There is a tendency for the observed subsidence to be slightly narrower than that predicted by the elastic theory which might suggest some inelasticity. The induced earthquakes themselves are the clearest evidence for inelastic deformation; however, the cumulative influence of the earthquakes on the measured surface deformation is negligible.

The stresses induced by gas extraction are consistent with the locations of the induced earthquakes if slip occurs on optimally oriented faults and the least principal stress is vertical. On the other hand, the predicted stressing together with slip on optimally oriented faults is inconsistent with the observed locations if the least principal stress is horizontal. Accurate determinations

of the fault plane solutions and in situ stress measurements would allow a more rigorous test of the poroelastic model and could place important constraints on the in situ stress state.

Appendix: Biot Coefficient and Pore Compressibility

The laboratory measurements [Vidal, 1988] determined the change in pore volume induced by a change in confining pressure at constant (atmospheric) pore pressure,

$$\left(\frac{\partial V_p}{\partial P_{conf}} \right)_p \tag{A1}$$

where V_p is the pore volume, P_{conf} is confining pressure, and p pore pressure. In the terminology of [Zimmerman et al., 1986], this is related to the compressibility C_{pc}, which is defined as

$$C_{pc} = -\frac{1}{V_p} \left(\frac{\partial V_p}{\partial P_{conf}} \right)_p \tag{A2}$$

The reciprocal theorem yields

$$\left(\frac{\partial V_b}{\partial p}\right)_{P_{conf}} = -\left(\frac{\partial V_p}{\partial P_{conf}}\right)_p \tag{A3}$$

where V_b is the bulk volume. The reciprocal relation can be written as

$$C_{pc} = \frac{1}{\phi}\frac{1}{V_b}\left(\frac{\partial V_b}{\partial p}\right)_{P_{conf}} \tag{A4}$$

where ϕ is porosity. Finally, the superposition principle gives

$$\frac{1}{V_b}\left(\frac{\partial V_b}{\partial p}\right)_{P_{conf}} = -\frac{1}{V_b}\left(\frac{\partial V_b}{\partial P_{conf}}\right)_p - \frac{1}{V_s}\left(\frac{\partial V_s}{\partial p}\right)_{P_{conf}=p} \tag{A5}$$

where V_s is the volume of the solid constituent [*Laurent et al.*, 1990]. This yields,

$$C_{pc} = \frac{1}{\phi}\left(\frac{1}{K} - \frac{1}{K_s}\right). \tag{A6}$$

Given that for homogeneous, isotropic solid constituent with fully connected pore space [*Nur and Byerlee*, 1971]

$$\alpha = 1 - \frac{K}{K_s} \tag{A7}$$

it follows that

$$\alpha = \phi K C_{pc}. \tag{A8}$$

References

Biot, M. A., General theory of 3-dimensional consolidation, *J. Appl. Phys.*, *12*, 155–164, 1941.

de Lanlay, J., Lacq profond-calage de l'historique sur le modele, *Elf Aquitane Technical report EP/S/PRO/GIN No E.90.020*, Pau, France, 1990.

Eason, G., B. Noble, and I. N. Sneddon, On certain integrals of Lipschitz-Hankel type involving products of Bessel functions, *Philos. Trans. R. Soc. London A*, *247*, 529–551, 1955.

Feignier, B., and J. R. Grasso, Seismicity induced by gas production, I, Correlation of focal mechanisms and dome structure, *Pure Appl. Geophys.*, *134*, 405–426, 1990.

Gallart, J., M. Daignieres, J. Gagnepain-Beyneix, and A. Hirn, Relationship between deep structure and seismicity in the western Pyrenees, *Annales Geophysicae*, *3*, 239–248, 1985.

Geertsma, J., Problems of rock mechanics in petroleum production engineering, in *Proceedings, First Congress International Society of Rock Mechanics, Lisbon: Labatorio Nacional de Engenharia Civil*, pp. 585–594. National Laboratory of Civil Engineering, Lisbon, Portugal, 1966.

Geertsma, J., Land subsidence above compacting oil and gas reservoirs, *J. Pet. Technol.*, *25*, 734–744, 1973.

Gephart, J. W., and D. W. Forsyth, An improved method for determining the regional stress tensor using earthquake focal mechanism data: Application to the San Fernando earthquake sequence, *J. Geophys. Res.*, *89*, 9305–9320, 1984.

Grasso, J. R., and B. Feignier, Seismicity induced by

gas production, II, Lithology correlated events, induced stresses and deformation, *Pure Appl. Geophys.*, *134*, 427–450, 1990.

Grasso, J. R., and G. Wittlinger, 10 years of seismic monitoring over a gas field area, *Bull. Seismol. Soc. Am.*, *80*, 450–473, 1990.

Guyoton, F., J.R. Grasso, and P. Volant, Interrelation between induced seismic instabilities and complex geologic structure, *Geophys. Res. Lett.*, *19*, 705–708, 1992.

Laurent, J., M. Bouteca, and J.P. Sarda, Pore pressure influence in the poroelastic behaviour of rocks: Experimental studies and results, in *EUROPEC90: Increasing the Margin; European Petroleum Conference*, pp. 385–392. Society of Petroleum Engineers, Richardson, Tex.,1990.

Nicolai, A., M. Pacaud, and A. Sitbon, Lacq gas field Aquitaine Basin France. in *Atlas of Oil and Gas Fields*, American Association of Petroleum Geologists, Tulsa, Okla., 1992.

Nur, A., and J.D. Byerlee, An exact effective stress law for elastic deformation of rock with fluids, *J. Geophys. Res.*, *76*, 6414–6419, 1971.

Pennington, W.D., S.D. Davis, S.M. Carlson, J.D. DuPree, and T.E. Ewing, The evolution of seismic barriers and asperities caused by the depressuring of fault planes in oil and gas fields of south Texas, *Bull. Seismol. Soc. Am.*, *76*, 939–948, 1986.

Reasenberg, P.A., and R. W. Simpson, Response of regional seismicity to the static stress changes produced by the Loma Prieta earthquake, *Science*, *255*, 1687–1690, 1992.

Rice, J.R., and M.P. Cleary, Some basic stress diffusion solutions for fluid-saturated elastic porous media with compressible constituents, *Rev. Geophys.*, *14*, 227–241, 1976.

Roeloffs, E.A., Fault stability changes induced beneath a reservoir with cyclic variations in water level, *J. Geophys. Res.*, *93*, 2107–2124, 1988.

Segall, P., Earthquakes triggered by fluid extraction, *Geology*, *17*, 942–946, 1989.

Segall, P., Induced stresses due to fluid extraction from axisymmetric reservoirs, *Pure Appl. Geophys.*, *139*, 535–560, 1992.

Stein, R. S., G.C.P. King, and J. Lin, Change in failure stress on the southern San Andreas fault system caused by the 1992 magnitude = 7.4 Landers earthquake, *Science*, *258*, 1328–1332, 1992.

Vidal, J., Mesure sous contraintes sur la 120, *Elf Aquitane Technical report EPS/S/PRO/RGI/PAU/JV/sj-no 125/88*, Pau, France, 1988.

Volant, P., Mecanisme des deformations et aspect fractal de la sismicite induite par l'exploitation d'un gisement d'hydrocarbures (Lacq, France), PhD Thesis, University of Grenoble, 158 pp., 1993.

Wetmiller, R.J., Earthquakes near Rocky Mountain House, Alberta and their relationship to gas production. *Can. J. Earth Sci.*, *23*, 172–181, 1986.

Yerkes, R.F. and R.O. Castle, Seismicity and faulting attributable to fluid extraction, *Engineering Geology*, *10*, 151–167, 1976.

Zimmerman, R.W., W.H. Somerton, and W.H. King, Compressibility of porous rocks, *J. Geophys. Res.*, *91*, 12,765–12,777, 1986.

J.R. Grasso, Laboratoire de Géophysique Interne et Tectonophysique, Observatoire de Grenoble, Grenoble, France.

A. Mossop, and P. Segall, Department of Geophysics, Stanford University, Stanford, CA 94305. (email:Internet segall@pangea.stanford.edu, mossop@pangea.stanford.edu)